IEEE Access
Multidisciplinary ⋮ Rapid Review ⋮ Open Access Journal

Received 30 January 2024, accepted 14 February 2024, date of publication 22 February 2024, date of current version 4 March 2024.

Digital Object Identifier 10.1109/ACCESS.2024.3368865

APPLIED RESEARCH

Heliostat Field Layout via Niching and Elite Competition Swarm Optimization

YANGHE ZOU[1], YIRAN ZHOU[2], AND QINGCHENG XU[3]
[1]School of Computer Science, Nanjing University of Information Science and Technology, Nanjing 210044, China
[2]Changwang School of Honors, Nanjing University of Information Science and Technology, Nanjing 210044, China
[3]School of Economics and Management, Nanjing Polytechnic Institute, Nanjing 210044, China

Corresponding author: Qingcheng Xu (xiqingcheng@njpi.edu.cn)

ABSTRACT Confronted with the challenges posed by climate change and the ongoing energy transition, solar energy is one of the important new energy sources, and the tower solar power plant has become an innovative solution to promote clean energy development. The optimization of heliostat field layout constitutes a crucial aspect in enhancing the operational efficiency of a concentrated solar power tower plant. Currently, the optimization of heliostat field layout has garnered widespread attention. In this paper, we propose the swarm optimization algorithm with niching and elite competition called NECSO to solve the large-scale heliostat field layout optimization. First, aiming to increase diversity and heterogeneity within the population, we employ a random grouping strategy to partition the population into distinct sub-swarms. Then, we design a niching and elite competition mechanism to harmonize the performance of the exploration. The niching competition is carried out within any sub-swarm to enhance the explorability of particles. The elite competition occurs between the elites which select from each sub-swarm to improve the convergence of particles. Additionally, we develop a mathematical model for the optimization of heliostat field layout. This model employs currently advanced computational methods, facilitating prompt and precise calculation of the optical efficiency in the heliostat field layout. To evaluate the performance of NECSO, we design 15 practical cases of heliostat field layout with varying scales. And then, we conduct comparative experiments with eight currently mainstream and excellent algorithms. The results indicate that NECSO exhibits competitive performance in solving the heliostat field layout optimization, particularly in large-scale cases.

INDEX TERMS Heliostat field layout, large-scale optimization, competitive swarm optimization, niching strategy.

I. INTRODUCTION

In recent years, the rapid surge in energy demand, paired with progressively stringent environmental regulations [1], has propelled the swift advancement of clean energy sources. Significant attention has been paid to tower solar thermal power plants, which is a representative of renewable energy technology. This technology stands out for its cleanliness, high efficiency, and energy storage capabilities, rendering it a pivotal choice for future energy demands [2]. The U.S. Department of Energy's (DOE) Office of Solar Energy Technology (SETO) launched the HelioCon Consortium and presented a roadmap study to advance heliostat technology [3], demonstrating the strategic value of solar thermal power plants.

A typical solar tower plant comprises various components, including heliostats, support structures, the receiving tower, heat transfer systems, thermal storage, and electricity generation components [4]. Among these, the heliostat field which concentrates sunlight onto a heat receiver positioned at the top of a tower is a critical subsystem of the solar tower plant. It often represents 50% of the total cost [5] and results in approximately 40% of power losses. Consequently, optimizing the layout of heliostats becomes a substantial challenge to enhance the overall efficiency.

The optical efficiency is a pivotal metric for evaluating a heliostat field [6]. However, a solar field with a heliostat typically comprises over 5000 heliostats [7], and each

The associate editor coordinating the review of this manuscript and approving it for publication was Poki Chen.

heliostat needs to have its optical efficiency calculated. This task imposes a considerable computational burden, exacerbated by the dimensional complexity introduced by size parameters and positional variables of the mirrors. Consequently, optimization algorithms must grapple with the challenges inherent in managing large-scale features [8], [9]. The high dimensionality of the problem results in an exponential expansion of the search space, leading to a pronounced degradation in the optimization performance of algorithms [10]. The arrangement of heliostats in the field significantly influences these optical indicators. Addressing the large-scale optimization of mirror field design becomes imperative for enhancing the energy efficiency of solar energy systems.

A. MODEL OF THE HELIOSTAT FIELD

Various models for heliostat field layouts have been developed since the late 1970s. Many researchers have explored the optical efficiency calculation and the design of heliostat field layouts.

Optical efficiency typically comprises reflection efficiency, cosine efficiency, interception efficiency, shading and blocking efficiency, and atmospheric transmission efficiency [11]. Among these, the shading and blocking efficiency are the key index of the optical efficiency. In the discretization model proposed by McFee [12], the mirror surface is partitioned into numerous small regions, and each region is scrutinized individually for shading to determine the blocking efficiency. However, a drawback of this approach is its high demand for computational resources. To address this drawback, the Sassi Method [13] employs solid analytic geometry. It minimizes the quantity of tests sent to the computer by determining overlapping portions through the division of the side faces of surface blocks rather than their areas. In addition, the method of using projection to calculate shading and blocking efficiency has gradually attracted the attention of researchers. In the CRS4-2 method [14], Leonardi and D'Aguanno calculated the projection of adjacent heliostats in the mirror direction and combine it with center distance filtering to obtain results. In 2014, Elayeb et al. [15] provided analytical expressions for the geometric shapes of projections and developed numerical iterative techniques for their solution. Other models, including HELIOS, MIRVAL, and DELSOL [16], [17], [18], have evolved into more contemporary software tools like SOLTRACE, FIATLUX, and HFLCAL [19], [20], [21]. Designers of heliostat fields can input parameters into these software tools to obtain optimized simulation results. However, in practical engineering projects, due to the diversity of scenarios and the complexity of heliostat fields, software simulations still incur significant time costs for optical efficiency calculations [22].

Building upon existing methods for optical efficiency calculations, researchers are also attempting to explore breakthroughs in heliostat field layout. They aim to find a heliostat field layout model that can be expressed using normalized parameters, transforming design optimization into adjustments of specific parameters and thus reducing the dimensionality of design variables. In 1978, [18] compared four common layouts, including radial cornfields, radial staggers, N.-S. cornfields, and N.-S. staggers. They concluded that the straggers model outperformed the cornfield model in terms of performance. Nevertheless, these models had constraints in reducing shadow losses arising from the overlapping of adjacent heliostats. To overcome this challenge, Collado and Guallar [23] introduced the "CAMPO" model in 2012, which features a radial staggered layout for the heliostat field. Furthermore, recent developments have explored biomimetic layouts inspired by principles from photosynthetic plants, such as using "phyllotaxis spiral patterns" [24] as a basis for heliostat layout. Through simulation and modeling, these patterns have proven effective in enhancing the system's optical efficiency. Belaid et al. [25] compared the performance of the CAMPO model and a biomimetic model using the heliostat field data from the PS10 solar power plant in Spain. They concluded that the CAMPO radial staggered layout exhibited better efficiency and minimized land usage. Furthermore, some researchers have proposed sequentially adding heliostat layout schemes and design layouts suitable for non-circular heliostat fields during the design process [26], [27].

In addition to the basic calculation of optical efficiency, the researchers also considered a number of factors that affect the energy conversion rate of Heliostats Feild. For example, the heliostat field of the ultra-high-concentration solar tower facility in Móstoles, Spain, has developed a contamination model [28] to reduce reflectance loss assessment time by combining measurements within the local heliostat and the average contamination ratio between different heliostats with different tilt angles. In addition, for the wind-induced heliostat tracking bias, an analytical model is proposed in [29], which can estimate and predict the wind-induced tracking bias with less computational resources. While [30] investigated the effectiveness of the mesh grid in the perimeter fence and edge mounting device of the heliostat field for reducing the wind load of the heliostat.

B. HELIOSTAT FIELD LAYOUT OPTIMIZATION METHODOLOGY

On the basis of determining the basic layout and heliostat field model, researchers have turned their attention to further optimizing heliostat fields. In the early days, the optimization of the layout of heliostat fields relied mainly on experimentation and experience. Engineers and researchers used an iterative trial-and-error approach to determine the angle and position of the heliostat to achieve optimal optical efficiency. This method was crude and relied on experience, resulting in inefficient of heliostat field. With the advancement of computer technology, various algorithms

TABLE 1. Overview of references.

Problem Statement	Year	Ref.	Authors	Method	Type
Biomimetic Heliostat Layout Optimization	2012	[24]	Corey J. Noone *et al.*	A new biomimetic placement	Non-heuristic
Multi-tower Heliostat Field Optimization Considering Heliostats Interactions	2016	[31]	Pasha Piroozmand *et al.*	PSO	Heuristic
Design of a Heliostat Field Based on the Gemasolar Plant	2019	[6]	Jianxing Wang *et al.*.	AGM-I and AGM-II	Non-heuristic
Pattern-free Heliostat Field Layout Optimization Using PS10 and a layout Obtained by SolarPILOT	2020	[32]	Seonghyeok Yang *et al.*	The Alternating Direction Method	Non-heuristic
Optimization of Heliostat Field Distribution Based on Delingha Tower Power Station	2021	[40]	Qiyue Xie *et al.*	An improved GWO	Heuristic
Heliostat Fields Optimization	2022	[33]	Victor Grigoriev *et al.*	Optimized the distribution of mirror density by solving a variational problem.	Non-heuristic
Estimating Shading and Blocking Losses in a Heliostat Field without Ray Tracing or Polygon Clipping	2022	[34]	Manish Raj *et al.*	A dual-filtering design.	Non-heuristic
Heliostat Field Optimization of Biomimetic Spiral and Radial-staggered layouts for Different Heliostat Shapes	2022	[25]	Abdelfetah Belaid *et al.*	The Grasshopper Optimization Algorithm (GOA)	Heuristic
Optimization of Biomimetic Heliostat Field	2022	[35]	Arslan A. Rizvi *et al.*	Advanced PSO, GA, WOA, GSA.	Heuristic
Solar Tower Heliostat Field Design Based on the Staggered Heliostat Field of the PS10 Plant	2022	[36]	Toufik Arrif *et al.*	GA, DE, PSO, GWO, ABC, GOA, IGWO, GA-GOA	Heuristic
Heliostat Wind Load Reduction	2022	[30]	Matthew J. Emes *et al.*	Investigation of the Mesh Grid Effectiveness	Non-heuristic
Multi-tower Ranging from 2 to 9 Towers Heliostat Field Optimization	2023	[37]	Lorenzo Pisani *et al.*	QUBO and quantum annealers.	Heuristic
A Highly-compact Heliostat Field	2023	[28]	Ricardo Conceição *et al.*	A Contamination Model	Non-heuristic
The Wind-induced Heliostat Tracking Bias	2023	[29]	Kristina Blume *et al.*	An Analytical Model	Non-heuristic
Engineering Heliostat Field Optimization	2023	[38]	Shuang Wang *et al.*	A Co-optimization Method	Heuristic
The Design of a Central Receiver Solar Thermal Power Plant	2023	[39]	Haris M *et al.*	GA Based on Rejection Sampling	Heuristic

have been introduced to address this problem. In mainstream optimization methods, they can be broadly categorized into two main types: non-heuristic algorithm optimization and heuristic algorithm optimization. Specifically, the references are shown in Table 1.

Non-heuristic algorithms focus on utilizing physical methods and mathematical techniques to narrow down the search space for optimization. AGM-I and AGM-II [40] are two concise yet accurate geometric analytic methods capable of identifying heliostats with the potential for shadowing or blocking, allowing for efficient recognition in heliostat fields. The alternating direction method [32] split the solar-weighted optical efficiency into two components: shading and blocking efficiency, non-shading and non-blocking efficiency. It then performed layout optimization based on physical gradients. To circumvent the high computational cost of ray tracing, Raj and Bhattacharya [34] designed a dual-filtering algorithm. This algorithm checks each grid from the edge to the center in a sequential manner, obtaining an approximate solution with lower computational cost. Grigoriev et al. [33], on the other hand, approached the problem from the perspective of heliostat density. They avoided parameter optimization and, instead, found the optimal distribution of heliostat density by solving a variational problem.

Heuristic algorithms, due to their inherent advantages in handling large-scale problems, can provide good solutions for parameter optimization in heliostat fields. In 2016, the Particle Swarm Optimization (PSO) algorithm was introduced to address the optimal layout problem in dual-tower heliostat fields [31]. Its optimization results showed certain advantages over other methods. In 2021, [40] proposed an enhanced Grey Wolf Optimization (GWO) algorithm based on the optical efficiency model for optimizing the parameters of heliostat fields. They improved the convergence factor and

weight updating formula, effectively avoiding local optimal issues. Building upon existing biomimetic spiral and Campo radial-staggered layouts, Belaid et al. [25] employed the Grasshopper Optimization Algorithm (GOA) to evaluate the efficiency of heliostat fields. Rizvi et al. [35] consolidated various advanced heuristic algorithms, including Particle Swarm Optimization, Genetic Algorithm, Whale Optimization Algorithm, and Gravity Algorithm, to accomplish the optimization process for biomimetic heliostat field design. Meanwhile, Arrif et al. [36] conducted a comparative analysis of eight metaheuristic algorithms approach to optimize the radial-staggered heliostat field at the PS10 plant, and a hybrid GA-GOA algorithm was proposed. This study presents the optimization process of a biomimetic heliostat field design using different heuristic optimization algorithms, namely advanced particle swarm optimization, genetic algorithm, whale optimization algorithm, and gravitational search algorithm. Additionally, The development of quantum computing has introduced new possibilities for algorithmic efficiency. Pisani et al. [37] utilized a quantum annealing algorithm in the Multi-tower model, revealing significant advantages over traditional annealing algorithms. Reference [38] combines engineering optimization and heuristic algorithm optimization to propose a co-optimization method based on coupling instantaneous optical, thermal and mechanical models, and then uses the obtained system model for design optimization based on genetic algorithm. A genetic algorithm (GA) based on rejection sampling [39] to optimize the field layout has also been applied to the heliostat field in Quetta, Pakistan, and this method has been shown to be effective in reducing the number of heliostats and improving efficiency.

C. CONTRIBUTION OF THIS WORK

In this paper, we endeavor to address the challenges associated with the large-scale optimization of heliostat layout. Initially, for rapid evaluation of the heliostat field layout, we constructed a model to assess the optical efficiency of the heliostat field. The model can accurately calculate the optical efficiency of the heliostat field in a limited time. Secondly, to enable the application of the heuristic algorithm in optimizing the heliostat field layout, we formulate a coding scheme for the problem. Lastly, optimizing the heliostat field layout presents a high-dimensional challenge as it requires simultaneous consideration of all heliostat positions. To mitigate the declining efficacy of heuristic algorithms in large-scale problems, we introduce the Niching and Elite Competition Swarm Optimization (NECSO) algorithm. Consequently, it efficiently and accurately addresses the large-scale optimization of heliostat field layout. Specifically, the contributions of this paper are as follows:

1) Optical efficiency modeling of heliostat field: The model contains almost all the metrics that affect the optical efficiency of the heliostat field. Additionally, to enhance algorithmic efficiency, we simplify metrics with minimal impact factors, such as specular reflectance and atmospheric transmittance. For metrics with substantial influence factors, we adhere rigorously to mathematical methods for derivation and calculation. Consequently, these endeavors enable the swift and accurate calculation of optical efficiency in large-scale heliostat fields.
2) Niching and elite competition swarm optimization: In our quest to enhance algorithmic performance in addressing large-scale problems, we introduce the Niching and Elite Competition Swarm Optimization (NECSO). First, we employ a random grouping strategy to partition the population into distinct sub-swarms. Subsequently, we devised a niching and elite competition mechanism to harmonize the exploratory and convergent aspects of particles. Niching competition occurs within each sub-swarm, where particles are randomly selected to compete, amplifying the exploratory characteristics of the particles. Elite competition transpires between sub-swarms, with each sub-swarm selecting the best particle as the elite participant for competition, thereby augmenting the convergence of the particles. Through these endeavors, the algorithm's performance in optimizing heliostat field layout is significantly enhanced.

We designed 15 cases to test the NECSO. At the same time, we compare the results with some classical heuristics and mathematical methods. The experimental results demonstrate that NECSO is competitive in solving the optimization of heliostat field layout, especially in the large-scale cases.

The remainder of the paper is organized as follows. Section II introduces the problem and the model for calculating optical efficiency. Section III delineates the competitive mechanism of the NECSO. Section IV describes the experimental cases, comparative algorithms, and experimental results. Section V analyses a small-scale case and convergence analysis. The final section summarizes the paper and presents future work.

II. PROBLEM STATEMENTS AND MATHEMATICAL MODELS

In this section, we first introduce the problem of heliostat field layout, then introduce the symbols used in this paper, and finally propose a mathematical model to solve the problem.

A. PROBLEM STATEMENTS

The area and geographical position of the heliostat field are known. In addition, we also know the height of the absorber and the height of the collector. Under the condition that the output thermal power of heliostat field reaches the standard, we need to design the number and position of heliostats so that the average optical efficiency of the heliostats field is maximum. Moreover, the problem to be solved has the following assumptions:

1) The heliostat sites are located in areas with flat terrain.
2) All the heliostats are in working order.

3) Each ray in the solar cone model carries the same amount of solar energy.

B. NOTIONS

R : radius of the heliostat field.
R_b : radius of plant layout centred on the absorption tower.
H_0 : height of absorption tower.
H_c : height of collector.
D_c : diameter of collector.
η : optical efficiency of the heliostat field.
η_{sb} : shadow occlusion efficiency.
$\eta_{\cos}$: cosine efficiency.
η_{at} : atmospheric transmittance.
η_{trunc} : truncation efficiency.
η_{ref} : reflectivity of mirrors.
DNI : the solar energy received by the surface of the earth per unit time when the sun's rays are perpendicular to a certain plane.
H : total number of heliostats.
L_W : width of the heliostat.
L_H : length of the heliostat.
h : mounting height of the heliostat.
hx_i : horizontal coordinates of the i-th heliostat.
hy_i : vertical coordinates of the i-th heliostat.
S : rated annual average output thermal power of heliostat field.
l_{max} : maximum value of the length of the heliostat.
l_{min} : minimum value of the length of the heliostat.
w_{max} : maximum value of width of the heliostat.
w_{min} : minimum value of width of the heliostat.

C. MATHEMATICAL MODELS

The η represents the optical efficiency of the heliostat field. In general, optical efficiency η is defined as follows [23], [31]:

$$\eta = \eta_{\text{sb}}\eta_{\cos}\eta_{\text{at}}\eta_{\text{trunc}}\eta_{\text{ref}} \tag{1}$$

Thermal output power of heliostat field E_{field} can be designed as follows:

$$E_{\text{field}} = \text{DNI} \cdot \sum_{i}^{N} A_i\eta_i \tag{2}$$

Atmospheric transmittance [41] η_{at} can be designed as follows:

$$\begin{aligned}\eta_{at} &= 0.99321 - 0.0001176d_{\text{HR}} \\ &\quad + 1.97 \times 10^{-8} \times d_{\text{HR}}^2 \quad (d_{\text{HR}} \le 1000)\end{aligned} \tag{3}$$

1) CALCULATION METHOD OF DNI

The solar altitude angle α_s calculation:

$$\sin\alpha_s = \cos\delta\cos\varphi\cos\omega + \sin\delta\sin\varphi \tag{4}$$

The solar azimuth γ_s calculation:

$$\cos\gamma_s = \frac{\sin\delta - \sin\alpha_s\sin\varphi}{\cos\alpha_s\cos\varphi} \tag{5}$$

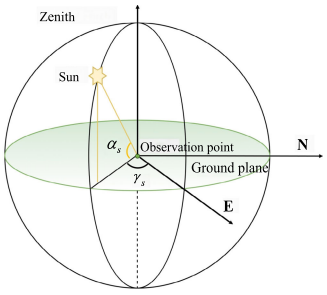

FIGURE 1. The solar altitude angle α_s and solar azimuth γ_s.

where, the north latitude of the circular heliostat field φ, the definition of the solar altitude angle α_s, and the definition of the solar azimuth γ_s are shown in Fig. 1.

The solar hour angle ω is calculated as follows:

$$\omega = \frac{\pi}{12}(ST - 12) \tag{6}$$

where, ST is the local time.

The solar declination angle δ is calculated as follows:

$$\sin\delta = \sin\frac{2\pi D}{365}\sin\left(\frac{2\pi}{360}23.45\right) \tag{7}$$

DNI can be approximated by the following formula:

$$\begin{aligned}\text{DNI} &= G_0\left[a + b\exp\left(-\frac{c}{\sin\alpha_s}\right)\right] \\ a &= 0.4237 - 0.00821(6 - H)^2 \\ b &= 0.5055 + 0.00595(6.5 - H)^2 \\ c &= 0.2711 + 0.01858(2.5 - H)^2\end{aligned} \tag{8}$$

2) COSINE EFFICIENCY CALCULATION MODEL

In order to ensure that the light reflected from the center of the heliostat points towards the center of the solar collector, it is necessary to continuously adjust the orientation of the heliostat in real-time, such that the incident sunlight direction is not perpendicular to the heliostat mirror surface but forms a certain angle with the incident light. This, in turn, results in a reduction of the projected surface area of the mirror in the direction of the vertical incident light. As a result, the effective radiation received by the heliostat is reduced, leading to cosine losses. Therefore, the key to calculating cosine efficiency lies in determining the angle of incidence based on the orientation of the heliostat.

For a single heliostat M_i (i represents the i-th heliostat in the heliostat field), without considering the thickness of the heliostat, if the center coordinate of its mirror is (x_i, y_i, h_i), h_i represents the installation height of the i-th heliostat, the horizontal and vertical coordinates of the center of the bottom surface of the absorption tower are (x_0, y_0), and H_0 is the height of the absorption tower. The height difference between $\Delta H_i = H_0 - h_i$. The distance between the center of the i-th heliostat and the center of the collector surface is $d_{HR,i} = \sqrt{(H_0 - h_i)^2 + d_{Hr,i}^2}$ and the projected distance

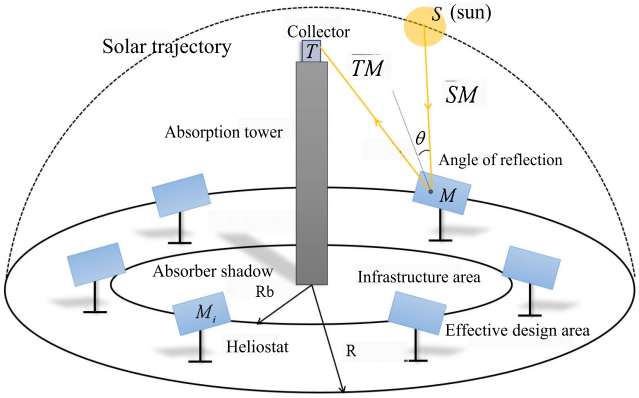

FIGURE 2. Cosine efficiency calculation model.

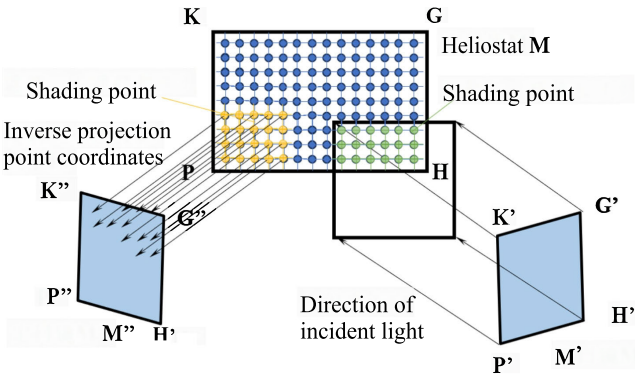

FIGURE 3. The shadow occlusion efficiency calculation model.

between two central points in the XOY plane is $d_{Hr,i} = \sqrt{(x_i - x_0)^2 + (y_i - y_0)^2} - \frac{D_c}{2}$.

The i-th heliostat azimuth ψ_i which represents the angle between the normal direction of the heliostat and the direction due south (XOZ plane) is calcuated as follows:

$$\psi_i = \arcsin(x_i + d_{HR,i}\cos\alpha_s \sin\gamma_s)/ \left(\sqrt{(x_i + d_{HR,i}\cos\alpha_s \sin\gamma_s)^2 + (y_i + d_{HR_i}\cos\alpha_s \cos\gamma_s)^2}\right) \tag{9}$$

The i-th heliostat pitch angle μ_i which represents the angle between the normal direction of the heliostat and the horizontal plane (XOY plane). is calcuated as follows:

$$\mu_i = \arccos \frac{d_{HR,i}\sin\alpha_s + \Delta H_1}{2 \cdot d_{HR,i}\cos\theta_i} \tag{10}$$

where, θ_i is the angle formed by the incident light of the sun and the normal vector of the i-th heliostat.

The angle of i-th heliostat tilt ρ_i which rpresents the angle between the normal direction of the heliostat and the YOZ plane is calcuated as follows:

$$\rho_i = \psi_i + \frac{\pi}{2} \tag{11}$$

Cosine efficiency refers to the ratio of the meridional cross section area and total area of the heliostat in the direction of the incident light due to the inclined incidence of sunlight, which is equal to the cosine value of the angle θ formed by the incident light and the normal vector of the heliostat. That is the cosine efficiency η_{cos}:

$$\eta_{cos} = cos\theta \tag{12}$$

where, the incident angle θ calculation diagram is shown in Figure 2. The formula is as follows:

$$\theta = \frac{1}{2}\arccos \frac{\overrightarrow{SM} \cdot \overrightarrow{TM}}{\left|\overrightarrow{SM}\right| \cdot \left|\overrightarrow{TM}\right|} \tag{13}$$

3) SHADOW OCCLUSION EFFICIENCY CALCULATION MODEL

In the construction of large-scale solar fields, shadowing efficiency is a critical parameter that influences the layout density of heliostats and the overall design of the solar field. Due to the possibility of both incident and reflected sunlight being obstructed by neighboring heliostats and the potential interception of sunlight by receiver towers during the incident process, this paper divides the shadow points during the incident process and the obstruction points during the reflection process to calculate the ineffective collection area on individual heliostat surfaces where sunlight cannot reach the collector.

A rectangular coordinate system was established with the center of the circular mirror field as the origin. The X-axis forward direction was due east, the Y-axis forward direction was due north, and the Z-axis forward direction was perpendicular to the ground. The calculation diagram of the area of shadow points and occluded points caused by shadow occlusion is shown in Fig. 3.

By solving the attitude parameters, solar azimuth angle γ_s and solar altitude angle α_s of the heliostat obtained, the coordinates of the intersection point between the solar incident light and the plane where the cross-section of the absorption tower is located are as follows:

$$\begin{cases} x_t = x - y \cdot \tan\gamma_s \\ y_t = 0 \\ z_t = z + y \cdot \dfrac{\tan\alpha_s}{\cos\gamma_s} \end{cases}$$

For a point (x, y, z) on a heliostat mirror, if its inverse projection corresponding to $(x_t, y_t, z_t) \in TOWER$, where $TOWER$ represents the point set formed by all points on the cross-section of the absorption tower, then the incident light at (x, y, z) is blocked by the absorption tower.

In the same way, the intersection of the sun incident light and its surface of the heliostat is:

$$\begin{cases} x' = x + \lambda \cdot \sin\gamma_s \\ y' = y + \lambda \cdot \cos\gamma_s \\ z' = z + \lambda \cdot \tan\gamma_s \end{cases}$$

where, λ is defined as follows:

$$\lambda = \frac{z + (y_j - y)\sin\rho_j \tan\mu_j - (x_j - x)\cos\rho_j \tan\mu_j}{\tan\alpha_s + \cos\gamma_s \sin\rho_j \tan\mu_j - \sin\gamma_s \cos\rho_j \tan\mu_j}$$

If $(x', y', z') \in \{M_j | j \neq i\}$, then the incident light at (x, y, z) is blocked by other heliostats. In total, the area of shadow points in the incident process of the i-th heliostat is $\sum \mathrm{d}S_{shad,i}$.

The light reflected by the mirror to the heat absorbing surface of the collector may be blocked by the heliostat near the tower on its inner side, so the solution method in the incident process is used to calculate any point (x, y, z) on the i th heliostat. The center coordinate of the rectangular mirror is $(x_i, y-i, z_i)$, and the center of the other mirror is $(x_j, y-j, z_j)$. The intersection point of the reflected light of a single mirror on the plane where the mirror of any other mirror is located can also be obtained:

$$\begin{cases} x'' = x + \lambda \cdot x_i \\ y'' = y + \lambda \cdot y_i \\ z'' = z + \lambda \cdot \Delta H_i \end{cases}$$

If $(x'', y'', z'') \in \{M_j | j \neq i\}$, then the reflected light at $(x, y, z)$is blocked by other heliostat. Thus, the sum of the area occupied by the occlusion point of the $i-th$ heliostat in the reflection process is obtained:$\sum \mathrm{d}S_{block,i}$.

Take $\sum \mathrm{d}S_{shad,i}$ and $\sum \mathrm{d}S_{block,i}$ two point set and set invalid lighting area of point set $\sum \mathrm{d}S_i$. Set the angle between the diagonal of the helioscope and its width to be β, and the rectangular area to be $2RM_i^2 \sin 2\beta_i$, thus the calculation formula of shadow occlusion efficiency η_{sb} is as follows:

$$\eta_{sb} = \frac{\sum \mathrm{d}S_i}{2RM_i^2 \sin 2\beta_i} \tag{14}$$

4) COLLECTOR TRUNCATION EFFICIENCY MODEL

The sunlight reflected by the heliostat is not completely concentrated to the collector, because in fact the sunlight itself is a beam of conical light with a certain angle, and any point of the reflected light on the heliostat is also a beam of conical light, which leads to a part of the sunlight scattered into the atmosphere, this scattering is called the truncation of the loss or overflow loss.

The solar cone is a figurative description of the process of concentrating light to a certain point with the sun's cross-section as the bottom disc of the cone, taking a light-gathering point on the mirror surface of the sun-setting mirror as the apex of the cone, and presenting two different cones to the direction of incidence and reflection. This paper does not separately discuss the truncation efficiency formula in the ''shadow blocking loss of energy'', but only to be able to reflect light from the mirror to judge the effectiveness of the collector heat absorption one by one. Collector truncation efficiency calculation schematic diagram in Fig. 4.

The equation of the collector in the ground level coordinate system is:

$$\begin{cases} x^2 + y^2 = R^2 \\ z \in [H_0 - \frac{h}{2}, H_0 + \frac{h}{2}] \end{cases} \tag{15}$$

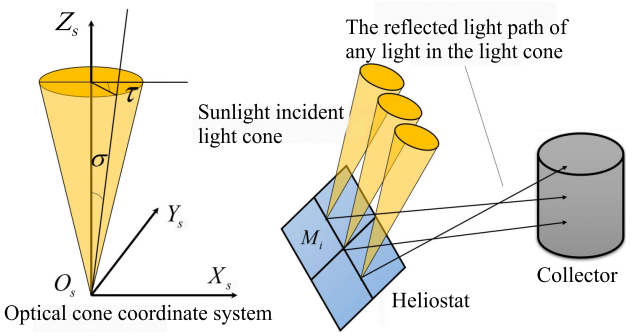

FIGURE 4. The collector truncation efficiency model.

For the solar incident light cone in the light that can be reflected from the mirror, solve the equation of the straight line where the reflected light is located, and the cylinder equation,. If the equation system has a solution, the energy of the light is absorbed by the collector, the collector produces an effective reception of energy E_{val}. Otherwise, it is an invalid light, and the ineffective energy dissipated is E_{inv}. In order to further observe the distribution of the energy flow density on the collector, the heat absorption area S_r on the columnar side of the collector is divided into a rectangular grid of $m \times n$, and the number of effective energy-absorbing intersections in each grid is counted, which is equivalent to the energy received by the collector in this grid.

For the grid matrix $F_{m\times n}$ in the i-th row and j-th column, if there are a total of K valid intersections in the grid, then the energy flow density $F_{i,j}$ is:

$$F_{i,j} = mn \cdot \frac{\sum_{k=1}^{K} \mathrm{d}E_k}{S_r} \tag{16}$$

The collector receives energy E_{val} as:

$$E_{val} = \sum F_{i,j} \cdot \frac{S_r}{mn} \tag{17}$$

The collector truncation efficiency η_{trunc} is calculated as:

$$\eta_{trunc} = \frac{E_{val}}{E_{val} + E_{inv}} \tag{18}$$

D. OBJECTIVES AND CONSTRAINTS

The objective function F is to maximize the optical efficiency of the heliostat field.

$$F = \max \eta \tag{19}$$

The constraint function C includes:

- Constraints on rated annual average output thermal power of heliostat field,

$$E_{field} \geq S \tag{20}$$

- Constraints on values for height and width of heliostats,

$$L_H \in [l_{min}, l_{max}], L_W \in [w_{min}, w_{max}] \tag{21}$$

- Constraints on values for the mounting height of heliostats,

$$h \geq \frac{L_W}{2} \tag{22}$$

- Constraints on the distance between heliostats,

$$sqrt((hx_i - hx_j)^2 + (hy_i - hy_j)^2) \geq min(w_i, w_j), \quad \forall i, j \in H, i \neq j \tag{23}$$

III. PROPOSED ALGORITHM

In recent research, certain scholars have addressed heliostat field layout optimization through linear programming or geometric approaches. Their objective is to develop easily computable methods applicable to multiple heliostat fields. However, this approach often results in decreased optical efficiency for certain heliostat fields, leading to resource wastage. This issue is particularly pronounced in large-scale heliostat fields. Therefore, in this paper, we propose niching and elite competition swarm optimization (NECSO). It utilizes the optical efficiency of a heliostat field as the optimization objective to maximize resource utilization.

In the subsequent subsections, we initially present a comprehensive overview of the overall framework, followed by an exposition on the competitive mechanisms involving niches and elites.

A. OVERALL PROBLEM-SOLVING FRAMEWORK

Algorithm 1 shows the overview framework of NECSO, and combining a niching and elite competition mechanism proposed in this paper based on competitive swarm optimization [42]. Before presenting the details of the framework process, the coding scheme of the algorithm is first introduced.

The coding scheme is a representation of the solution to the problem, and it is also critical to the efficiency of the algorithm. The coding scheme of the NECSO consists of two parts. The first part represents the attribute of the heliostat, which is common to all heliostats. The second part is the coordinates of each heliostat. All the parts have a total of $2n + 4$ elements. In the first part, L_H represents the length of the heliostat, L_W represents the width of the heliostat, h represents the mounting height of the heliostat, and n represents the number of heliostats. In the first part, all the basic parameters of the heliostat are included. The second part represents the coordinates of the heliostats, which is the key part to be optimized, this part is extremely important for the optical efficiency of the heliostat field. In general, this coding scheme makes the problem solving well carried out.

The details of NECSO are as follows. First, we initialize the population to obtain a set of candidate solutions (line 1). References [43] and [44] indicates that the quality of the initial population can improve the performance of population-based stochastic search algorithms. Therefore, we use layout based on Campo [23] to initialize the layout of the heliostat field to make the initialised population closer to the optimal solution. Then, we evaluate the fitness of each particle (line 2) and finally optimize the layout of the heliostat field by the NECSO (line 3 - line 9). At each iteration, we randomly divide the particles into k sub-swarm (line 4). Subsequently particles update velocity and position with niching competition (line 5) and elite competition (line 6). Finally, we limit the position and velocity of each particle (line 7) and evaluate each particle (line 8). The flowchart illustrating the solution to the optimization of the heliostat field layout is depicted in Fig.5.

Algorithm 1 The Niching and Elite Competition

1: Initialize the population P.
2: Evaluate each particle in population P.
3: **while** Termination conditions not met **do**
4: Randomly divide the population P into k niches.
5: The niching competition (Algorithm 2).
6: The elite competition in (Algorithm 3).
7: Limit the velocity and position of each particle.
8: Evaluate each particle in population P.
9: **end while**

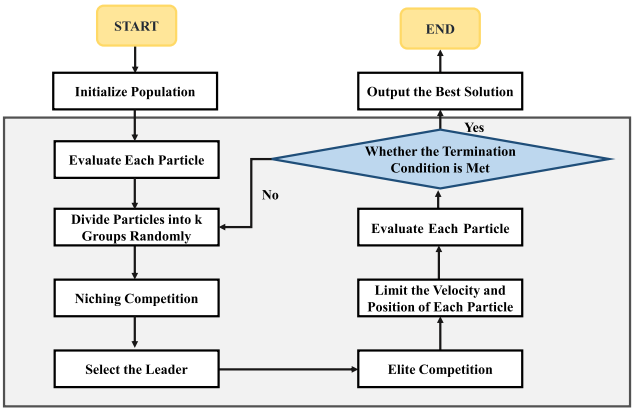

FIGURE 5. The flowchart for the heliostat field layout optimization.

B. THE NICHING AND ELITE COMPETITION MECHANISM

To balance the population diversity and convergence, we propose a niching and elite competition combined with CSO to solve the heliostat field layout. NECSO is divided into niching competition and elite competition. As shown in Fig. 6, first, we use a random grouping strategy [45] to divide the population into sub-swarm. Then, the competition within the niching enhances the exploration ability of particles, and elite competition makes the population convergence speed increase. The specific niching competition mechanism and elite competition mechanism are described below.

1) THE NICHING COMPETITION

Each particle engages in competition with others within the niching. Initially, each particle is sequentially chosen within the niching. Subsequently, a particle is randomly selected in the niching for the competition. Particle positions and

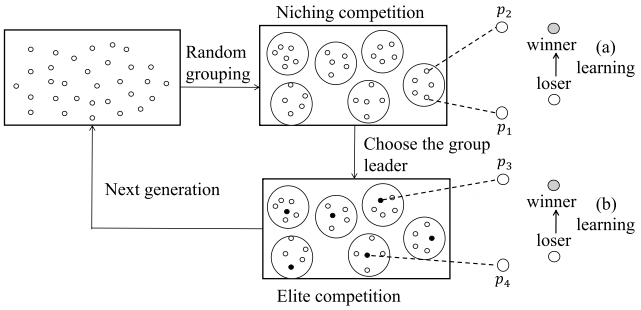

FIGURE 6. The niching and elite competition mechanism. (a) Indicates competition within the niching. (b) Indicates elite competition. The losers learn from the winners.

velocities are updated according to equations (24) and (25). The purpose of the random grouping is to increase the diversity of the population, and the competition within the niching makes the exploration space of the particles expand further. The specific implementation of the niching competition is detailed in Algorithm 2.

$$v_{nl,t+1} = r_1 v_{nl,t} + r_2(x_{nw,t} - x_{nl,t}) + \varphi r_3(\overline{x_1} - x_{nl,t}), \quad (24)$$

$$x_{nl,t+1} = x_{nl,t} + v_{nl,t+1}, \quad (25)$$

where $r_1, r_2, r_3 \in [0, 1]^D$ are three random vectors following a uniform distribution, $\overline{x_1}$ is the average position of all particles in the sub-swarm, φ is a parameter used to control the effect of $\overline{x}$, x_{nw} and v_{nw} denote the position and velocity of the winning particle in the sub-swarm, and x_{nl} and v_{nl} denote the position and velocity of the losing particle in the sub-swarm.

Algorithm 2 The Niching Competition

for each niching m in total nichings **do**
  for each particle i in the niching m **do**
    Randomly select particle j in the niching
    if $fitness_i \geq fitness_j$ **then**
      Update the velocity and position of i and j.
      Winner's collection $P_1 \leftarrow i$.
      Loser's collection $P_2 \leftarrow j$.
    else
      Update the velocity and position of i and j.
      Winner's collection $P_1 \leftarrow j$.
      Loser's collection $P_2 \leftarrow i$.
    end if
  end for
end for

2) THE ELITE COMPETITION

For each niching, we choose the elites in each niching to compete. First, we choose the best fitness particle in each sub-swarm to be the elite. Subsequently for each elite, one from the set of elites is randomly selected for competition. Finally, the particles update the velocity and position by Eqs. (26)(27). The elite competition allows the better particles to learn from each other, which leads to faster convergence of the population. The detail of elite competition is illustrated in Algorithm 3.

$$v_{el,t+1} = r_1 v_{el,t} + r_2(x_{ew,t} - x_{el,t}) + \varphi r_3(\overline{x_2} - x_{el,t}), \quad (26)$$

$$x_{el,t+1} = x_{el,t} + v_{el,t+1}, \quad (27)$$

where $\overline{x_2}$ is the average position of all particles in the elite, x_{ew} and v_{ew} denote the position and velocity of the winning particle in the elite, and x_{el} and v_{el} denote the position and velocity of the losing particle in the elite.

Algorithm 3 The Elite Competition

for each niching i in total nichings **do**
  Finding the best particle in niching i.
  The elite's collection $L \leftarrow i$.
end for
for each particle i in the elite's collection L **do**
  Randomly select particle j in the niching
  if $fitness_i \geq fitness_j$ **then**
    Update the velocity and position of i and j.
    Winner's collection $P_1 \leftarrow i$.
    Loser's collection $P_2 \leftarrow j$.
  else
    Update the velocity and position of i and j.
    Winner's collection $P_1 \leftarrow j$.
    Loser's collection $P_2 \leftarrow i$.
  end if
end for

IV. NUMERICAL EXPERIMENTS

This section conducts testing of the NECSO across 15 distinct heliostat field sizes. Initially, detailed data for the test cases is presented. Subsequently, we describe the comparison algorithms, concluding with the presentation of experimental results. The algorithms are implemented and executed using MATLAB 2023a. Execution of the algorithms takes place on a Mac computer featuring a 2.3GHz Core i7 processor and 16GB RAM. The code for NECSO can be found at https://github.com/EvoNexusX/2024ZouNECSO.

A. CASE GENERATION

To validate the validity and accuracy of our proposed model and algorithm, we generated 15 different cases. The parameters for these cases are presented in Table 2, where C_1-C_5 represent small-scale cases, C_6-C_{10} represent medium-scale cases, and C_{11}-C_{15} represent large-scale cases.

Additionally, the heliostat's length, L_H, varies within the range of [2, 6], while the width, L_W, is constrained to [2, 4]. The height of the tower, H_0, is fixed at 80m. The collector is characterized by an external cylindrical light-receiving structure with a height, H_c, of 8m and a diameter, D_c, of 7m. The heliostat field is positioned at 40 degrees north latitude and 100 degrees east longitude.

To enhance the accuracy of optical efficiency calculations, we select five specific time points each day: 8:00, 10:00,

TABLE 2. Parameters for the 15 cases used to test the algorithm.

Case	$R(m)$	$R_b(m)$	$S(MW)$
C_1	350	100	40
C_2	350	100	45
C_3	350	100	50
C_4	350	100	55
C_5	350	100	60
C_6	550	150	50
C_7	550	150	50
C_8	550	150	60
C_9	550	150	70
C_{10}	550	150	80
C_{11}	700	200	90
C_{12}	700	200	110
C_{13}	700	200	130
C_{14}	700	200	150
C_{15}	700	200	170

12:00, 14:00, and 18:00. We then compute the average optical efficiency across these moments to determine the daily optical efficiency of the heliostat field. On a monthly basis, we choose the 1st, 10th, 20th, and 30th days to calculate a four-day average, representing the optical efficiency for that month. Subsequently, we calculate the yearly average optical efficiency and utilize it as the optical efficiency for the heliostat field.

B. COMPARISON ALGORITHMS

To showcase the advantages of NECSO in addressing the optimization of a heliostat field layout, we devised a comparative experiment. The algorithms for comparison encompass six heuristic algorithms and a mathematical planning algorithm, each described as follows.

1) CSO [42]: CSO is particularly well-suited for handling large-scale problems owing to the competitive nature of its particles, which exhibit high exploratory capabilities. In this study, CSO serves as a comparison algorithm, specifically utilized to assess and contrast the large-scale performance of NECSO.
2) PSO [46]: PSO demonstrates rapid convergence. In low-dimensional problems, PSO is known for its swift convergence and ability to easily identify the global optimal solution. In this research, the algorithm serves as a comparative benchmark, employed to illustrate and evaluate the convergence performance of NECSO.
3) GA [47]: GA is a classical heuristic algorithm known for its robust global search capabilities. GA, by retaining multiple solutions and iteratively enhancing them through genetic operations, typically exhibits a strong ability to explore the global solution space. In this study, GA is employed as a comparative algorithm to illustrate and assess the global search capability of NECSO.
4) CAMPO [23]: CAMPO employs a mathematical programming model to optimize the layout of the heliostat field. In this research, CAMPO serves as a comparative algorithm to highlight the advantages of the heuristic algorithm NECSO in addressing the optimization challenge associated with the heliostat field layout.
5) HSJOA [48]: HSJOA is a variant of Joint operations algorithm (JOA) based on hierarchical structure with excellent performance in global optimization problems. This paper employs it as a benchmark algorithm for comparative analysis.
6) PSE-DE [49]: PSE is an enhanced framework based on population state evaluation. This paper incorporates PSE into differential evolution(DE) [50] as a comparative algorithm.
7) DCDE [51]: DCDE is a novel variant of DE, based on dynamic composite mutation operators and a two-level parameter adjustment strategy. DCDE demonstrates strong performance in optimizing global problems, and this paper utilizes it as a benchmark algorithm for comparative analysis.

The running parameters of all the algorithms are shown in Table 3. In addition, each algorithm has the same number of evaluations, $200*n$, in each testing round. Each test case runs with different random numbers ten times.

TABLE 3. Parameters of the algorithms.

Algorithm	The running parameters settings
NECSO	$k = 10, \varphi = 0.1, NP = 2 \cdot D$
CSO	$\varphi = 0.1, NP = 2 \cdot D$
PSO	$W = 0.729, c_1 = 2.05 \cdot W, c_2 = 2.05 \cdot W, NP = 2 \cdot D$
GA	$P_c = 0.8, P_m = 0.2, NP = 2 \cdot D$
HSJOA	$C_{NU} = 6, C_{EP} = 18$
PSE-DE	$F = 0.7, CR = 0.5, IT = 250, AT_{init} = 0.02, NP = 5 \cdot D$
DCDE	$NP = 2 \cdot D$

C. RESULTS DISPLAY

We conduct experimental tests based on the aforementioned cases, and the specific results are presented in Table 4. The values bolded in the table indicate that the algorithm is the optimal choice under these specific circumstances. The penultimate line, denoted as (+/=/−) represents the comparative results between seven algorithms and NECSO. "+" denotes that NECSO outperforms the algorithm, "=" indicates that NECSO performs equally to the algorithm, and "−" signifies that NECSO is inferior to the algorithm. The final line provides the ranking of all algorithms in this experiment through the Friedman test [52]. For clarity in presenting the results, Figure 7 illustrates the best-fit values of the eight algorithms and the standard deviation of the seven heuristic algorithms.

Upon analyzing Table 4, it is evident that NECSO outperforms the other seven algorithms, trailing behind only in cases C_2, C_3, C_6, C_9, C_{10} and C_{14}. In the small-scale cases (C_1-C_5), the slower convergence of particles in NECSO is attributed to the competition within the niching,

TABLE 4. Best fitness obtained by the eight algorithms under the same evaluation model and compared with NECSO.

Case	NECSO	CSO	PSO	GA	HSJOA	PSE-DE	DCDE	CAMPO
C_1	**7.47E-01**	7.39E-01	7.42E-01	7.20E-01	**7.47E-01**	7.45E-01	**7.47E-01**	7.10E-01
C_2	7.36E-01	7.35E-01	7.44E-01	7.12E-01	**7.46E-01**	7.32E-01	7.45E-01	7.05E-01
C_3	7.36E-01	7.22E-01	**7.38E-01**	6.83E-01	7.35E-01	7.31E-01	7.33E-01	6.96E-01
C_4	**7.29E-01**	7.23E-01	7.22E-01	6.82E-01	7.21E-01	7.19E-01	7.21E-01	6.88E-01
C_5	**7.16E-01**	7.15E-01	7.04E-01	6.79E-01	7.10E-01	7.14E-01	7.11E-01	6.85E-01
C_6	7.05E-01	6.89E-01	6.97E-01	6.69E-01	**7.06E-01**	6.99E-01	7.05E-01	6.53E-01
C_7	**6.99E-01**	6.83E-01	6.74E-01	6.68E-01	6.95E-01	6.85E-01	6.89E-01	6.49E-01
C_8	**6.98E-01**	6.80E-01	6.58E-01	6.37E-01	6.92E-01	6.80E-01	6.78E-01	6.45E-01
C_9	6.91E-01	6.63E-01	6.59E-01	6.34E-01	6.90E-01	**6.92E-01**	6.78E-01	6.40E-01
C_{10}	6.70E-01	6.49E-01	6.53E-01	6.20E-01	6.72E-01	6.70E-01	**6.75E-01**	6.36E-01
C_{11}	**6.61E-01**	6.33E-01	5.78E-01	6.07E-01	6.54E-01	6.52E-01	6.54E-01	5.26E-01
C_{12}	**6.48E-01**	6.13E-01	5.75E-01	5.87E-01	6.21E-01	6.19E-01	6.22E-01	5.23E-01
C_{13}	**6.34E-01**	6.14E-01	5.79E-01	5.78E-01	6.15E-01	6.17E-01	6.17E-01	5.18E-01
C_{14}	6.03E-01	**6.05E-01**	5.71E-01	5.67E-01	5.86E-01	5.98E-01	6.01E-01	5.15E-01
C_{15}	**5.99E-01**	5.90E-01	5.71E-01	5.50E-01	5.85E-01	5.84E-01	5.89E-01	5.11E-01
Ranking	1.73	4.30	5.20	7.27	2.93	3.97	3.00	7.30
$+/=/-$		14/0/1	13/0/2	15/0/0	11/1/3	14/0/1	11/2/2	15/0/0

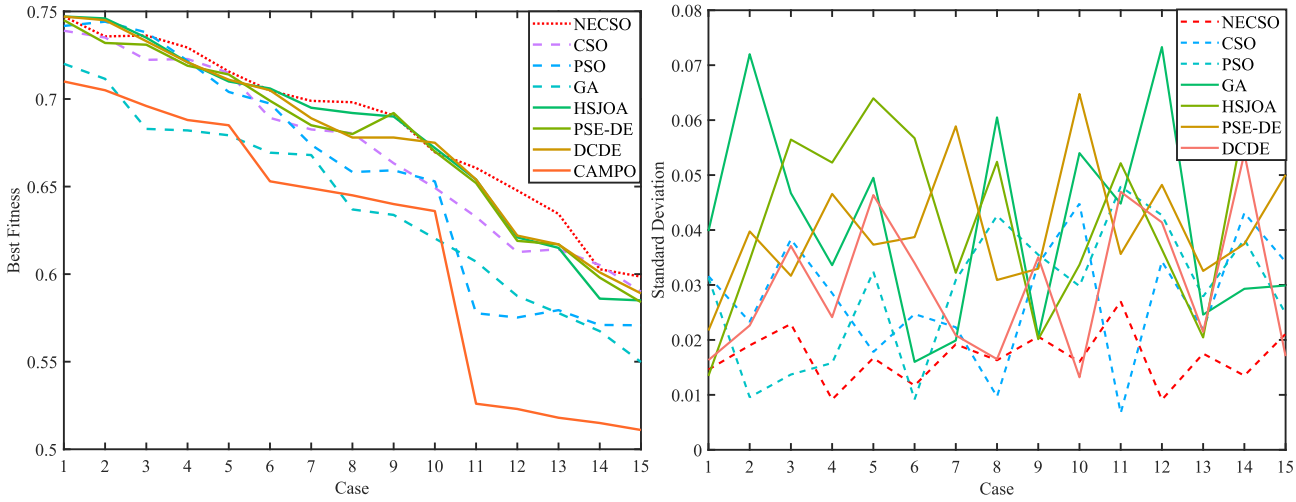

(a) Best fitness for the eight algorithms.

(b) Standard deviation of seven heuristic algorithms.

FIGURE 7. Best fitness for eight algorithms and standard deviation of the seven heuristic algorithms.

which enlarges the search space. This phenomenon results in slightly lower performance in cases C_2 and C_3. In the case of middle-scale cases (C_6-C_{10}), In cases C_6 and C_{10}, NECSO falls behind HSJOA, while in case C_9, it lags behind PSE-DE. Additionally, in case C_{10}, NECSO trails behind DCDE. In the case of large-scale cases (C_{11}-C_{15}), competition among elites enables NECSO to converge faster than CSO. Consequently, NECSO outperforms CSO in the majority of cases, with only a slight lag observed in C_{14}. Overall, NECSO demonstrates superior performance across all cases, with a minimal performance gap even in cases where it lags behind.

Comparing NECSO with the other seven algorithms, especially with the mathematical planning algorithm CAMPO, reveals NECSO's superior performance, particularly in larger-scale cases. This can be attributed to the strong environmental adaptability of the heuristic algorithm. In comparison with CAMPO, it exhibits robust performance, particularly in larger-scale heliostat fields. CSO is designed to address large-scale problems, but due to the competition among elites in NECSO, leading to faster convergence, NECSO outperforms CSO in small to medium-scale cases. PSO, a classical particle swarm algorithm, tends to fall into local optima. As the problem size increases, PSO's performance rapidly declines. NECSO's niching competition mechanism expands particle search space, reducing the likelihood of falling into local optima, significantly outperforming PSO in medium and large-scale problems. GA, a classical heuristic algorithm, performs poorly for high-dimensional problems like optimizing the heliostat field layout, lagging far behind NECSO. Despite HSJOA, PSE-DE, and DCDE being currently high-performing heuristic algorithms, their

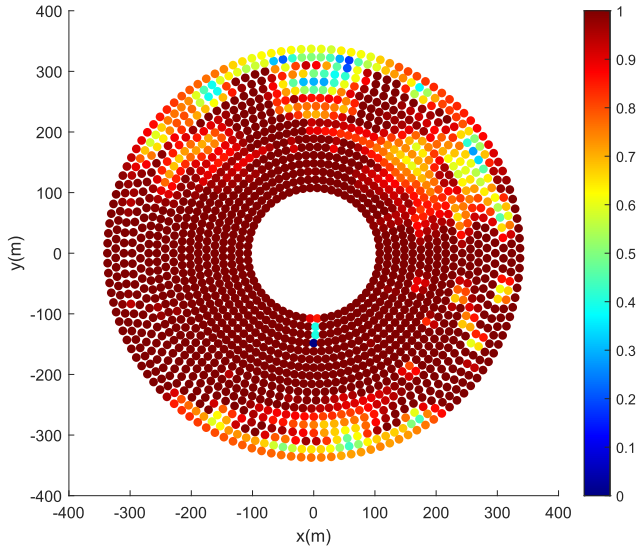

FIGURE 8. Shading Efficiency in heliostat fields at 2:00 PM Beijing time.

performance tends to decline when confronted with problems of dimensions in the order of thousands.

In the Friedman test, NECSO achieved a ranking of 1.73, surpassing the other algorithms. The algorithm that follows NECSO closely is HSJOA, with a ranking of 2.93. CAMPO had the lowest ranking at 7.30. This demonstrates the superiority of NECSO in addressing large-scale heliostat fields.

Additionally, some noteworthy conclusions emerge. Heuristic algorithms consistently outperform the mathematical planning algorithm CAMPO, with GA being the only exception, lagging behind CAMPO in some small and medium-scale cases. HSJOA, PSE-DE, and DCDE, as the currently high-performing algorithms, outperform CSO, PSO, and GA in terms of their performance. Furthermore, NECSO and CSO maintain their superior performance over other algorithms when addressing ultra-large-scale problems.

In summary, NECSO exhibits significantly higher overall performance and stability than the other seven algorithms across various cases.

V. DISCUSSION

In this section, we first analyse the correctness of the NECSO in solving the problem. Then we discuss the NECSO convergence speed. Finally, we analyze the experimental parameters and results.

A. A CASE STUDY

In this section, we select case C_1 for validation to ensure the accuracy of our proposed model. The shading efficiency is a crucial component of the optical efficiency calculation. We specifically computed the shading efficiency at 2:00 PM Beijing time in the local afternoon, as illustrated in Fig. 8.

In Fig. 8, the visual representation indicates a clear shadow cast by the tower, and the shading efficiency of the heliostat field exhibits symmetry about the absorption tower. This

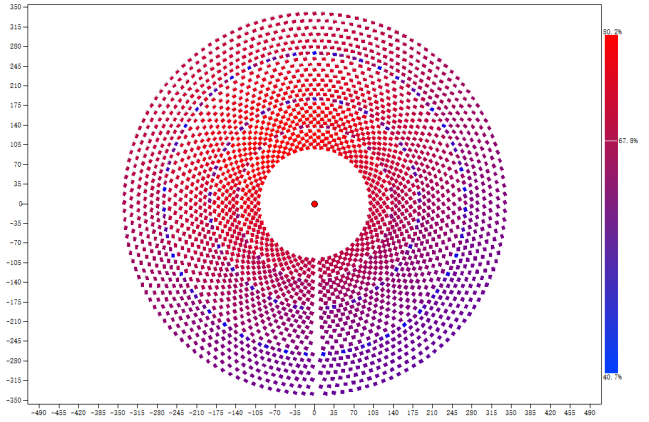

FIGURE 9. Initial layout of the heliostat field.

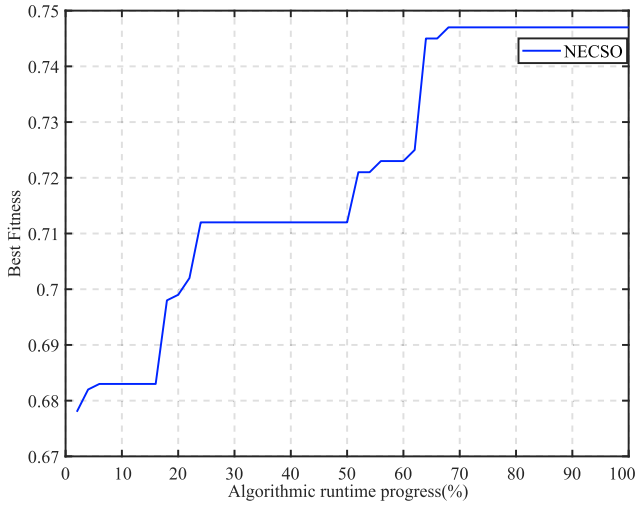

FIGURE 10. The convergence curve for this case.

observation closely aligns with the outcomes of light-cone modeling. Consequently, the model demonstrates a high level of accuracy in calculating the shading efficiency.

The initial layout of the NECSO is depicted in Fig. 9, representing a standard interphase layout model. Notably, a strategic design choice involves reducing the number of heliostats in the shadow of the tower, aiming to enhance the overall optical efficiency of the heliostat field. The calculated optical efficiency for this initial layout is 0.678.

Fig. 10 illustrates the optimization curve for NECSO. As the iterations progress, the optimal adaptation value steadily increases until convergence. The solution for this case is determined by selecting the best particle from the last generation.

Our analysis of case C_1 demonstrates that NECSO consistently moves toward the anticipated objective at each step in problem-solving. In summary, the reliability of NECSO in addressing this problem can be confidently affirmed.

B. CONVERGENCE ANALYSIS

In this section, we analyze the convergence of NECSO using a comparison shown in Fig. 11. We select two cases

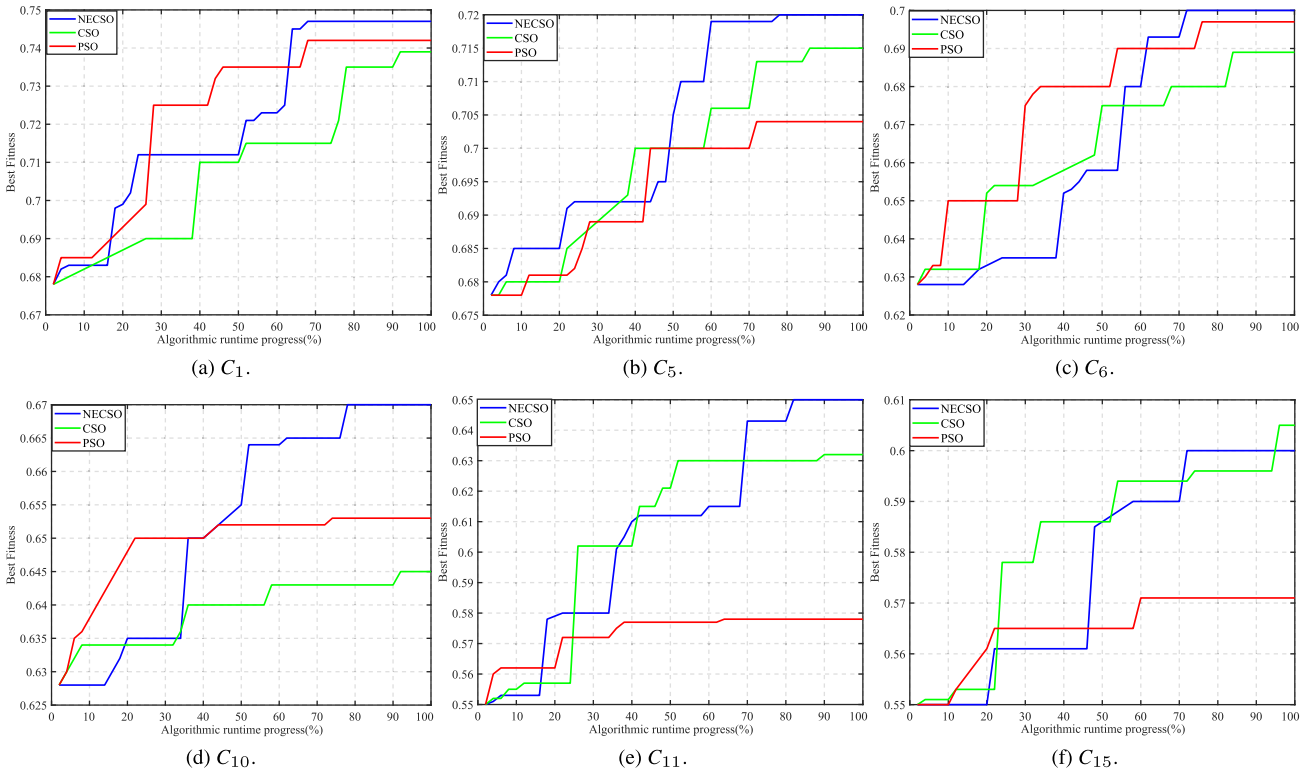

(a) C_1. (b) C_5. (c) C_6.

(d) C_{10}. (e) C_{11}. (f) C_{15}.

FIGURE 11. Convergence curves for three algorithms.

in each scale, totaling six cases. The horizontal axis of each graph indicates the progression of algorithmic runtime, while the vertical axis represents the best adaptation value corresponding to each generation.

As depicted in Fig. 11, NECSO, CSO, and PSO all begin with the same initial value to ensure a fair comparison. In small-scale cases (C_1 and C_5), NECSO converges much faster than CSO, attributed to the competition between elites that enables a quick population convergence, making NECSO superior to CSO. Although the convergence speed of NECSO is slower than PSO, the particles in NECSO exhibit greater exploratory behavior, resulting in an overall superior performance compared to PSO.

In medium and large scales, the strong exploratory nature of particles in NECSO and CSO becomes evident. PSO, on the other hand, converges prematurely in medium and large-scale problems, leading to suboptimal solutions. In contrast to CSO, NECSO demonstrates accelerated convergence, markedly enhancing the quality of the optimal solution achieved within a constrained number of iterations.

In general, the convergence speed of NECSO lies between that of CSO and PSO. The niching and elite competition mechanisms in NECSO strike a balance between exploratory and convergent properties of particles, resulting in better overall performance compared to CSO and PSO.

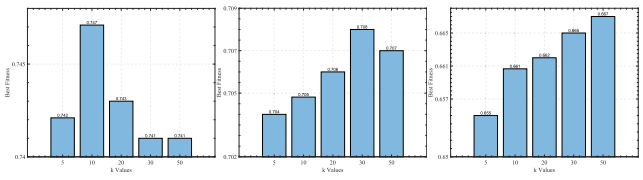

(a) C_1. (b) C_6. (c) C_{11}.

FIGURE 12. For a given value of φ equal to 0.1, the best fitness of each cases under different values of k.

C. PARAMETER ANALYSIS

In the NECSO, there are two crucial parameters, i.e, φ and k. Extensive experiments in [42] demonstrate that the optimal empirical value for φ is 0.1. In this section, we analyze the impact of different values of k on the optimal fitness of cases through experiments. We selected representative cases C_1, C_6, and C_{11} from various scales, with k values set to 5, 10, 20, 30, and 50.

Fig. 12 represents the impact of different k values on the optimal fitness of cases. The values of k have a certain impact on cases of different scales, but the influence is not significant, with only a small difference observed. In the small-scale case C_1, the best solution is obtained when k is set to 10. However, in the large-scale case C_{11}, the optimal solution is achieved with k set to 50. As the problem scale increases, the range of solution distribution becomes broader. With more particles in the groups, NECSO's search space expands. Therefore, larger values of k lead to higher-quality solutions.

TABLE 5. Results obtained by the Wilcoxon test for algorithm NECSO.

VS	R^+	R^-	Exact P-value	Asymptotic P-value
CSO	117.0	3.0	≥ 0.2	0.001005
PSO	114.5	5.5	≥ 0.2	0.001654
GA	120.0	0.0	≥ 0.2	0.00059
HSJOA	89.0	16.0	≥ 0.2	0.015624
PSE-DE	104.0	1.0	≥ 0.2	0.000912
DCDE	104.0	16.0	≥ 0.2	0.010352
CAMPO	120.0	0.0	≥ 0.2	0.000539

D. STATISTICAL ANALYSIS

In this section, we employed the Wilcoxon test [53] for non-parametric statistical analysis, and the analysis results are presented in the table as shown in Table 5. VS represents the comparison between NECSO and the algorithms in the table. R^+ represents the extent to which NECSO outperforms the respective algorithm. A higher R^+ value implies superior performance on certain problems. R^- represents the extent to which an algorithm performs less favorably than NECSO. A higher R^- value may suggest relatively poorer performance on other problems.

The Table 5 indicates that NECSO demonstrates statistically significant superiority over the compared algorithms. For instance, when compared to CSO, NECSO exhibits a substantial R^+ value of 117.0, implying a significant outperformance. Similar patterns are observed with PSO, GA, HSJOA, PSE-DE, DCDE, and CAMPO, where NECSO consistently achieves higher R^+ values, indicating superior performance across a range of problems. The P-values further validate the statistical significance of these findings, with most Exact and Asymptotic P-values being less than 0.05.

In summary, the results of the Wilcoxon test demonstrate the outstanding performance of NECSO in addressing the optimization of heliostat field layout.

Based on the experimental results and analysis, NECSO shows excellent performance in optimizing large-scale heliostat field layout. The experimental numerical analysis further proves the superiority of NECSO. Compared to the other seven algorithms, especially in large-scale cases, NECSO shows higher convergence speed and superior solution quality. Firstly, the niching competition mechanism ensures diversity within different types of particles in the niches, expanding the search space of particles and preventing premature convergence to local optima in large-scale cases. Secondly, the leader competition mechanism accelerates the convergence of the population by fostering competition among elite individuals, ensuring the entire population converges more rapidly to superior solutions. This guarantees effective performance not only in large-scale scenarios but also in medium and small-scale problems. Through these competitive mechanisms, NECSO achieves a balanced performance across various problem scales, excelling not only in large-scale cases but also demonstrating commendable capabilities in medium and small-scale scenarios.

Despite the advantages of NECSO in optimizing the layout of heliostat fields, the model and algorithm still have certain limitations, as follows:

1) In the model section, we assumed that all components in the heliostat field would operate normally, without considering the impact of uncertainties in the environment. For instance, we did not consider scenarios where some heliostats are damaged or where geographical factors may result in the malfunctioning of certain heliostats.
2) In the algorithmic section, firstly, NECSO demonstrates suboptimal performance in certain problem instances, potentially influenced by the initial parameter settings and characteristics of the problems, resulting in considerable performance fluctuations. This is attributed to the varied optimal values of parameters such as φ and k arising from diverse problem characteristics, impacting the algorithm's overall efficacy. Secondly, under specific circumstances, NECSO may exhibit slower convergence rates compared to other algorithms, particularly evident in small-scale problems. This phenomenon stems from the limited number of evaluations in small-scale problems, where internal competition within niches impedes the population from converging effectively. These limitations underscore the necessity for more refined tuning or enhancements in NECSO, particularly in varying problem scales, to bolster its robustness and performance.

VI. CONCLUSION

This paper has introduced the niching and elite competition swarm optimization (NECSO) algorithm as a novel approach to tackle the optimization challenges associated with large-scale heliostat field layout. Our methodology encompasses several key steps. Firstly, we have established a comprehensive model for evaluating the optical efficiency of the heliostat field, providing a foundation for quick and accurate calculations. Subsequently, designed to harmonize the explorability and convergence of particles is a mechanism incorporating both niching and elite competition. The core of our contribution lies in the NECSO mechanism. This algorithm incorporates a new strategy, utilizing niching competition to enhance particle explorability and elite competition to expedite particle convergence. The niching competition operates within sub-swarms, fostering diversity and exploration, while elite competition occurs between different sub-swarms, promoting convergence towards optimal solutions. Finally, in our experimental evaluation, we have compared the performance of NECSO against several mainstream heuristic algorithms. The results demonstrate the superior efficacy of NECSO across various cases,especially in large-scale, showcasing its ability to outperform these established algorithms. Importantly, NECSO exhibits stability and correctness even in small-scale

cases, further establishing its versatility and reliability in addressing heliostat field layout optimization challenges.

In the future, our research will explore large-scale heliostat field optimization in uncertain environments. Additionally, we aim to extend the application of NECSO to other domains such as blockchain problems [54], global optimization problems [55], and distributed computing problems [56].

REFERENCES

[1] L. Gan, "Energy development and environmental constraints in China," *Energy Policy*, vol. 26, no. 2, pp. 119–128, Feb. 1998.

[2] Z. Wang, "Prospectives for China's solar thermal power technology development," *Energy*, vol. 35, no. 11, pp. 4417–4420, Nov. 2010.

[3] G. Zhu, C. Augustine, R. Mitchell, M. Muller, P. Kurup, A. Zolan, S. Yellapantula, R. Brost, K. Armijo, J. Sment, R. Schaller, M. Gordon, M. Collins, J. Coventry, J. Pye, M. Cholette, G. Picotti, M. Arjomandi, M. Emes, D. Potter, and M. Rae, "HelioCon: A roadmap for advanced heliostat technologies for concentrating solar power," *Sol. Energy*, vol. 264, no. 1, Nov. 2023, Art. no. 111917.

[4] S. Alexopoulos and B. Hoffschmidt, "Advances in solar tower technology," *Wiley Interdiscipl. Rev., Energy Environ.*, vol. 6, no. 1, p. e217, 2017.

[5] G. J. Kolb, S. A. Jones, M. W. Donnelly, D. Gorman, R. Thomas, R. Davenport, and R. Lumia, "Heliostat cost reduction study," Sandia Nat. Laboratories, Albuquerque, NM, USA, Tech. Rep. SAND2007-3293, 2007, vol. 103.

[6] J. Wang, L. Duan, Y. Yang, and L. Yang, "Rapid design of a heliostat field by analytic geometry methods and evaluation of maximum optical efficiency map," *Sol. Energy*, vol. 180, pp. 456–467, Mar. 2019.

[7] A. F. Hildebrandt and L. L. Vant-Hull, "Power with Heliostats: A central receiver illuminated by a field of heliostats can absorb 10 to 100 megawatts of sunlight at 600° to 1000° K," *Science*, vol. 197, no. 4309, pp. 1139–1146, 1977.

[8] P. Xu, W. Luo, X. Lin, J. Zhang, Y. Qiao, and X. Wang, "Constraint-objective cooperative coevolution for large-scale constrained optimization," *ACM Trans. Evol. Learn. Optim.*, vol. 1, no. 3, pp. 1–26, Sep. 2021.

[9] P. Xu, W. Luo, X. Lin, Y. Chang, and K. Tang, "Difficulty and contribution-based cooperative coevolution for large-scale optimization," *IEEE Trans. Evol. Comput.*, vol. 27, no. 5, pp. 1355–1369, Oct. 2023.

[10] P. Xu, W. Luo, X. Lin, J. Zhang, and X. Wang, "A large-scale continuous optimization benchmark suite with versatile coupled heterogeneous modules," *Swarm Evol. Comput.*, vol. 78, Apr. 2023, Art. no. 101280.

[11] J. Abatut and A. Achaibou, "Analysis and design of a field of heliostats for a solar power plant," *Sol. Energy*, vol. 21, no. 6, pp. 453–463, 1978.

[12] R. McFee, "Computer program CONCEN for calculation of irradiation of solar power central receiver," in *Proc. ERDA Solar Workshop Methods Opt. Anal. Central Receiver Syst.* Houston, TX, USA: Univ. of Houston, 1977, pp. 197–213.

[13] G. Sassi, "Some notes on shadow and blockage effects," *Sol. Energy;(United Kingdom)*, vol. 31, no. 3, Jan. 1983.

[14] E. Leonardi and B. D'Aguanno, "CRS4-2: A numerical code for the calculation of the solar power collected in a central receiver system," *Energy*, vol. 36, no. 8, pp. 4828–4837, Aug. 2011.

[15] M. E. Elayeb, R. A. Haman, and F. M. Siala, "Calculation of the blocking factor in heliostat fields," *Energy Proc.*, vol. 57, pp. 291–300, Jan. 2014.

[16] P. Garcia, A. Ferriere, and J.-J. Bezian, "Codes for solar flux calculation dedicated to central receiver system applications: A comparative review," *Sol. Energy*, vol. 82, no. 3, pp. 189–197, Mar. 2008.

[17] A. Kribus, R. Zaibel, D. Carey, A. Segal, and J. Karni, "A solar-driven combined cycle power plant," *Sol. Energy*, vol. 62, no. 2, pp. 121–129, Feb. 1998.

[18] F. Lipps and L. Vant-Hull, "A cellwise method for the optimization of large central receiver systems," *Sol. Energy*, vol. 20, no. 6, pp. 505–516, 1978.

[19] T. Wendelin, "SolTRACE: A new optical modeling tool for concentrating solar optics," in *Proc. Int. Sol. Energy Conf.*, vol. 36762, 2003, pp. 253–260.

[20] L. P. Tidbury, G. Czanner, and D. Newsham, "Fiat Lux: The effect of illuminance on acuity testing," *Graefe's Arch. Clin. Exp. Ophthalmol.*, vol. 254, pp. 1091–1097, Apr. 2016.

[21] P. Schwarzbözl, R. Pitz-Paal, and M. Schmitz, "Visual HFLCAL—A software tool for layout and optimisation of heliostat fields," in *Proc. 15th Int. SolarPACES Symp.*, Berlin, Germany, Sep. 2009, pp. 15–18.

[22] M. Sánchez and M. Romero, "Methodology for generation of heliostat field layout in central receiver systems based on yearly normalized energy surfaces," *Sol. Energy*, vol. 80, no. 7, pp. 861–874, 2006.

[23] F. J. Collado and J. Guallar, "Campo: Generation of regular heliostat fields," *Renew. Energy*, vol. 46, pp. 49–59, Oct. 2012.

[24] C. J. Noone, M. Torrilhon, and A. Mitsos, "Heliostat field optimization: A new computationally efficient model and biomimetic layout," *Sol. Energy*, vol. 86, no. 2, pp. 792–803, Feb. 2012.

[25] A. Belaid, A. Filali, S. Hassani, T. Arrif, M. Guermoui, A. Gama, and M. Bouakba, "Heliostat field optimization and comparisons between biomimetic spiral and radial-staggered layouts for different heliostat shapes," *Sol. Energy*, vol. 238, pp. 162–177, May 2022.

[26] Y. Yao, Y. Hu, and S. Gao, "Heliostat field layout methodology in central receiver systems based on efficiency-related distribution," *Sol. Energy*, vol. 117, pp. 114–124, Jul. 2015.

[27] X. Wei, Z. Lu, W. Yu, and Z. Wang, "A new code for the design and analysis of the heliostat field layout for power tower system," *Sol. Energy*, vol. 84, no. 4, pp. 685–690, Apr. 2010.

[28] A. M. H. Ricardo Conceição, "Experimental soiling assessment, characterization and modelling of a highly-compact heliostat field in an urban environment," *Sol. Energy*, vol. 262, Sep. 2023, Art. no. 111812.

[29] K. Blume, M. Röger, and R. Pitz-Paal, "Full-scale investigation of heliostat aerodynamics through wind and pressure measurements at a pentagonal heliostat," *Sol. Energy*, vol. 251, pp. 337–349, Feb. 2023.

[30] M. J. Emes, A. Jafari, and M. Arjomandi, "A feasibility study on the application of mesh grids for heliostat wind load reduction," *Sol. Energy*, vol. 240, pp. 121–130, Jul. 2022.

[31] P. Piroozmand and M. Boroushaki, "A computational method for optimal design of the multi-tower heliostat field considering heliostats interactions," *Energy*, vol. 106, pp. 240–252, Jul. 2016.

[32] S. Yang, K. Lee, and I. Lee, "Pattern-free heliostat field layout optimization using physics-based gradient," *Sol. Energy*, vol. 206, pp. 722–731, Aug. 2020.

[33] V. Grigoriev, K. Milidonis, C. Corsi, and M. Blanco, "Heliostat fields with a balanced mirror density," *Sol. Energy*, vol. 243, pp. 336–347, Sep. 2022.

[34] M. Raj and J. Bhattacharya, "An accurate and cheaper method of estimating shading and blocking losses in a heliostat field through efficient filtering, removal of double counting and parallel plane assumption," *Sol. Energy*, vol. 243, pp. 469–482, Sep. 2022.

[35] A. A. Rizvi, D. Yang, and T. A. Khan, "Optimization of biomimetic heliostat field using heuristic optimization algorithms," *Knowl.-Based Syst.*, vol. 258, Dec. 2022, Art. no. 110048.

[36] T. Arrif, S. Hassani, M. Guermoui, A. Sánchez-Gonzâlez, R. A. Taylor, and A. Belaid, "GA-GOA hybrid algorithm and comparative study of different metaheuristic population-based algorithms for solar tower heliostat field design," *Renew. Energy*, vol. 192, pp. 745–758, Jun. 2022.

[37] L. Pisani, G. S. Moreau, E. Leonardi, C. Podda, A. Mameli, and G. Cao, "Multi-tower heliostat field optimization by means of adiabatic quantum computer," *Sol. Energy*, vol. 263, Oct. 2023, Art. no. 111893.

[38] S. Wang, C.-A. Asselineau, A. Fontalvo, Y. Wang, W. Logie, J. Pye, and J. Coventry, "Co-optimisation of the heliostat field and receiver for concentrated solar power plants," *Appl. Energy*, vol. 348, Oct. 2023, Art. no. 121513.

[39] M. Haris, A. U. Rehman, S. Iqbal, S. O. Athar, H. Kotb, K. M. AboRas, A. Alkuhayli, and Y. Y. Ghadi, "Genetic algorithm optimization of heliostat field layout for the design of a central receiver solar thermal power plant," *Heliyon*, vol. 9, no. 11, 2023, Art. no. e21488.

[40] Q. Xie, Z. Guo, D. Liu, Z. Chen, Z. Shen, and X. Wang, "Optimization of heliostat field distribution based on improved Gray Wolf optimization algorithm," *Renew. Energy*, vol. 176, pp. 447–458, Oct. 2021.

[41] O. Farges, J.-J. Bézian, and M. El Hafi, "Global optimization of solar power tower systems using a Monte Carlo algorithm: Application to a redesign of the PS10 solar thermal power plant," *Renew. Energy*, vol. 119, pp. 345–353, Apr. 2018.

[42] R. Cheng and Y. Jin, "A competitive swarm optimizer for large scale optimization," *IEEE Trans. Cybern.*, vol. 45, no. 2, pp. 191–204, Feb. 2015.

[43] P. Xu, W. Luo, J. Xu, Y. Qiao, J. Zhang, and N. Gu, "An alternative way of evolutionary multimodal optimization: Density-based population initialization strategy," *Swarm Evol. Comput.*, vol. 67, Dec. 2021, Art. no. 100971.

[44] P. Xu, W. Luo, J. Xu, Y. Qiao, and J. Zhang, "Density-based population initialization strategy for continuous optimization," in *Bio-Inspired Computing: Theories and Applications*. Singapore: Springer, 2021, pp. 46–59.
[45] Y. Sun, P. Xu, Z. Zhang, T. Zhu, and W. Luo, "Brain storm optimization integrated with cooperative coevolution for large-scale constrained optimization," in *Proc. 14th Int. Conf. Swarm Intell. (ICSI)*. Cham, Switzerland: Springer, 2023, pp. 356–368.
[46] J. Kennedy and R. Eberhart, "Particle swarm optimization," in *Proc. Int. Conf. Neural Netw. (ICNN)*, vol. 4, Nov./Dec. 1995, pp. 1942–1948.
[47] S. Mirjalili, "Genetic algorithm," in *Evolutionary Algorithms and Neural Networks*. Cham, Switzerland: Springer, 2019, pp. 43–55.
[48] G. Sun, R. Han, L. Deng, C. Li, and G. Yang, "Hierarchical structure-based joint operations algorithm for global optimization," *Swarm Evol. Comput.*, vol. 79, Jun. 2023, Art. no. 101311.
[49] C. Li, G. Sun, L. Deng, L. Qiao, and G. Yang, "A population state evaluation-based improvement framework for differential evolution," *Inf. Sci.*, vol. 629, pp. 15–38, Jun. 2023.
[50] R. Storn and K. Price, "Differential evolution—A simple and efficient heuristic for global optimization over continuous spaces," *J. Global Optim.*, vol. 11, pp. 341–359, Dec. 1997.
[51] L. Deng, C. Li, Y. Lan, G. Sun, and C. Shang, "Differential evolution with dynamic combination based mutation operator and two-level parameter adaptation strategy," *Expert Syst. Appl.*, vol. 192, Apr. 2022, Art. no. 116298.
[52] J. Derrac, S. Garcia, L. Sanchez, and F. Herrera, "KEEL data-mining software tool: Data set repository, integration of algorithms and experimental analysis framework," *J. Multiple-Valued Logic Soft Comput.*, vol. 17, no. 2, pp. 255–287, 2015.
[53] D. Rey and M. Neuhäuser, "Wilcoxon-signed-rank test," in *International Encyclopedia of Statistical Science*. Berlin, Germany: Springer, 2011, pp. 1658–1659.
[54] M. Nour, J. P. Chaves-Ávila, and Á. Sánchez-Miralles, "Review of blockchain potential applications in the electricity sector and challenges for large scale adoption," *IEEE Access*, vol. 10, pp. 47384–47418, 2022.
[55] M. Qaraad, S. Amjad, N. K. Hussein, S. Mirjalili, N. B. Halima, and M. A. Elhosseini, "Comparing SSALEO as a scalable large scale global optimization algorithm to high-performance algorithms for real-world constrained optimization benchmark," *IEEE Access*, vol. 10, pp. 95658–95700, 2022.
[56] M. Dolatabadi, P. Siano, and A. Soroudi, "Assessing the scalability and privacy of energy communities by using a large-scale distributed and parallel real-time optimization," *IEEE Access*, vol. 10, pp. 69771–69787, 2022.

YANGHE ZOU is currently pursuing the degree with Nanjing University of Information Science and Technology, Nanjing, China. His research interest includes large-scale global optimization algorithms and applications.

YIRAN ZHOU is currently pursuing the degree with Nanjing University of Information Science and Technology, Nanjing, China. Her research interest includes large-scale global optimization algorithms and applications.

QINGCHENG XU received the master's degree in accounting from Nanjing University, in 2015. She is currently a Lecturer with the School of Economics and Management, Nanjing Polytechnic Institute. Her main research interests include optimization, supply chain management, and management accounting.